Article

Comparison of AC Losses in the Winding of Electrical Machines with Fixed Strands Positions, Fixed Conductor Shapes and Random Winding

Anuvav Bardalai [1],[†] , David Gerada [1],[*],[†] , Tianjie Zou [1],[†], Michele Degano [1],[†], Chengming Zhang [2],[†] and Chris Gerada [1]

1   Power Electronics, Machines and Control Group (PEMC), University of Nottingham, Nottingham NG7 2RD, UK
2   Department of Electrical Engineering, Harbin Institute of Technology, Harbin 150000, China
*   Correspondence: d.gerada@nottingham.ac.uk
†   These authors contributed equally to this work.

Abstract: In high performance electric machines, the increase of fundamental frequency leads to additional losses in the winding due to parasitic effects such as the associated skin and proximity effects. In the first part, this paper presents an investigation into accurate modelling of AC losses in the winding using numerical methods and their experimental verification. Then, using experimental motorette setups, this research provides a comparative study between fixed strand positioning and fixed conductor shapes on the AC losses in the winding. It is shown that the exact position of strands in the conductor is not a critical factor; however, it is very important to control the conductor shape inside the slot. In the final section of this paper, an investigation into the relationship between AC losses in the winding and copper filling factor is presented. It is shown experimentally that counter-intuitive design choices such as using a lower copper fill factor and thicker strand diameters may be beneficial in achieving the highest overall efficiency.

Keywords: AC copper loss; circulating currents; permanent magnet machines; proximity effect; windings

1. Introduction

One of the main challenges the contemporary world faces is the increased transport energy demands leading to increased emissions and global warming. To counter these challenges, governments globally are introducing stringent emissions standards and international regulations, spanning land, air and marine transportation [1]. Car manufacturers have chosen to address these targets by incorporating electric motors within the drivetrains [2]. Electric vehicles (EVs) such as plug-in hybrid electric vehicles (PHEVs) and battery electric vehicles (BEVs) boost energy efficiency by using high efficiency electric drive systems and contribute to a wide range of transport goals such as enhanced energy security, better air quality and less noise together with reduced greenhouse gas emissions. Hence, the demand for electric machines with a step-change improvement in performance metrics (kW/kg, kW/L, $/kW) have become an important R&D topic, with various national bodies such as the DoE in the US and the Advanced Propulsion Centre (APC) in the UK setting up ambitious targets [3]. A straightforward solution for reducing the size of the machines is to increase the rotational speed and hence the fundamental frequency of the machines [4,5]. In fact, recent automotive traction drives have motors rotating with speeds as high as 20 krpm. In BEVs, most of the commercial solutions for the power traction system use permanent magnet synchronous motors (PMSM) with embedded rare-earth magnets [6–8]. This is because of the combination of several advantages such as high efficiency, high power factor, high torque density, high overload capability, robustness, reduced maintenance,

compactness and low weight of PMSM. The flux-weakening capability of the PMSM allows for operating in a wider range of speed.

The trend to increase the maximum rotational speed and hence the fundamental frequency gives rise to more pronounced parasitic phenomena, mainly skin and proximity effects. In low-voltage machines with a smaller turn count, the conductors are split into smaller individual strands connected in parallel. This results in an uneven current distribution across the strands and causes circulating currents to flow. The result of the aforesaid effects is the increase in the effective resistance of the windings in the machine and thus an increase in the power loss. With the stator winding losses making up most of the power loss in high-power-density electric machines [9], reducing the winding copper losses becomes a matter of importance.

The parasitic AC losses in the windings of high-speed electric machines are a well-researched area [5,10–18], and several antidotes have been presented. For a given operational frequency, selecting a strand diameter smaller than the skin penetration-depth and using several thinner strands in parallel is one of such countermeasures to reduce AC losses in the winding. This, however, does not eliminate the proximity effects which still exist since parallel paths for coil turns located in the slot top and slot bottom have different flux linkages between them due to higher leakage flux at the slot top. In light of this, another commonly applied measure in high frequency machines is to keep the area in close proximity to the slot opening, where higher leakage flux occurs, unwound [10,19–21]. Twisting/transposing a coil along the slot length [13,22,23] or using litz wire [24–27] are the other options that reduce the AC losses. Twisted strands reduce the slot-filling factor, which increase the DC copper losses, while litz wire, apart from reducing the fill factor, is expensive in comparison to the relatively inexpensive round magnet wires. In [18], it is shown that by carefully controlling the positions of the strands within the top of the slot, the AC losses can be significantly reduced.

This paper delves further into the research presented in [18]. Using numerical methods, it provides an investigation into accurate modelling of winding AC losses together with experimental verification of the models. Experimental motorette setups are used to conduct a comparative study between fixed strands' positions (as presented in [18]) and fixed conductor shapes on the AC losses in the winding. Furthermore, an experimental investigation into the relationship between AC losses in the winding and copper filling factor is presented in this research.

The paper is organized as follows: Section 2 introduces the machine under investigation and its numerical modelling for AC loss calculation. Section 3 presents the comparison of FE analysis results and the results of the representative experimental motorette. In Section 4, comparative analysis between fixed strands positions and fixed conductor shapes is performed. Section 5 presents an experimental investigation into the relationship between AC losses in the winding and copper filling factor, and Section 6 shows the segregation of winding loss into its components. Finally, conclusions of this research are summarized in Section 7.

2. Machine Specification and Methodology

An existing EV traction machine, the details of which are listed in Table 1, is used for the analysis in this paper. The machine-rated power is 37 kW, with a wide constant power speed range (CPSR). The base speed is 2800 rpm, while the maximum speed is 23 krpm, corresponding to a fundamental frequency of 1.5 kHz

Table 1. Machine parameter and specification.

Parameter	Specification
Machine type	3-ph. IPMSM
Rated Power	37 kW
Rated/Peak Speed	2800/23,000 rpm
Winding type	2 layers concentrated
Strand type	Round Magnet wire
Strands-in-hand	33
Strand Diameter	0.704 mm
Strand nominal diamter	0.63 mm
Slot filling factor	0.42

2.1. Finite-Element (FE) Modelling

For the purpose of this research, a motorette setup is modelled in finite element analysis (FEA) as shown in Figure 1(left). Since, the actual machine has a double layer concentrated winding, the motorette is modelled with three slots and two coils. A strand nominal diameter of 0.8 mm is used with nine strands-in-hand. Table 2 lists the details of the motorette. Figure 1(right) shows the half side of a slot in the motorette with strands' and conductors' positions. The different colors represent the different turns and the numbers highlighted in green represent the conductors/turns' positions in the slot. Discs of the same color represent parallel strands or 'strands-in-hand' of a conductor. In FEA, the strands are modelled as solid conductors and are connected in the external circuit to form parallel strands and turns. Figure 2 shows the circuital representation of the strands and turns connections corresponding to the motorette. The 2D FE analysis is carried out for the DC current as well as for various fundamental frequencies of up to 1500 Hz.
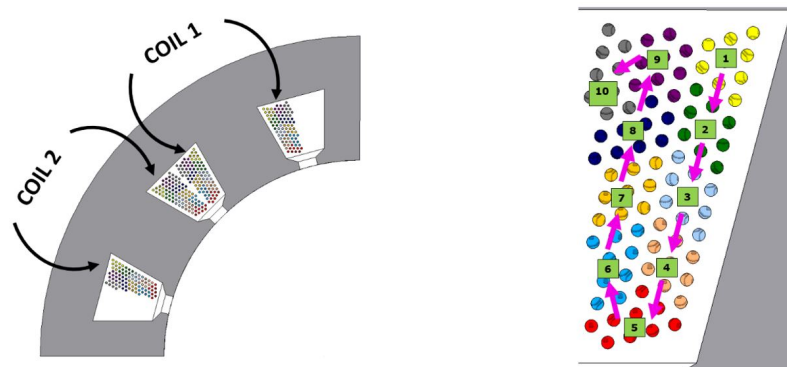

Figure 1. (**Left**) Finite element model of the machine motorette with strand-level winding. (**Right**) Representation of conductor layout and positions in the half side of a slot of the motorette.

Table 2. Motorette parameter and specification.

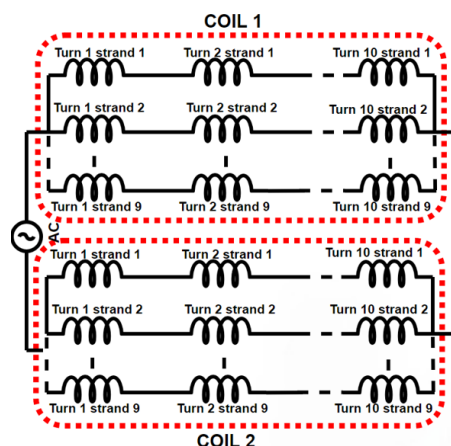| Parameter	Specification
Winding type	Concentrated
Layers	2
Turns per slot	20
Strands-in-hand	9
Strand type	Round Magnet Wire
Strand diameter	0.834 mm
Strand nominal diameter	0.8 mm

Figure 2. Representation of circuital connections of strands and turns in the motorette model.

2.2. Experimental Motorette

Utilising precision 3D printing, a slot former was manufactured with holes that precisely match the strand positions in the FEA simulations. Figure 3 shows a slot former used for fixing the strand positions. The strands were then meticulously wound in the experimental motorette to match the exact positions of each strand in the FEA, as shown in Figure 4.
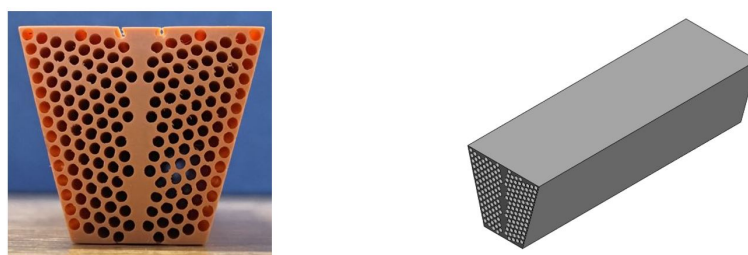

Figure 3. Slot former used for the experimental motorette: (**Left**) 3D printed slot former; (**Right**) 3D render of the slot former.

Figure 4. One wound coil in the experimental motorette with the slot former inserted.

The motorette was fed with an AC power source (Chroma Programmable AC source) which can supply variable frequencies, and a precision power analyser (PPA 5530 from N4L) was used to measure the losses in the motorette. Figure 5 shows the schematic of the experimental setup, and Figure 6 shows the actual experimental setup. To ascertain that all the measurements are taken at the same temperature, thermocouples were inserted in the slot former to give the real-time temperature inside the slot. A current of 30 A_{rms} was used for all analysis in this paper. The AC resistances of the auxiliary components (connecting wires, supply cables) were measured using a precision impedance analyser (E4990A from KEYSIGHT technologies, Santa Rosa, CA, USA). Figure 7 shows the measured AC resistance of the connecting wire against the frequency, measured up to 2 kHz. Since the resistance of the auxiliary components does not change significantly with an increase in frequency,

they are considered as DC values, and the losses in these components are considered as DC losses. Furthermore, as with the preceding research presented in [18], no AC losses are assumed to occur at the end-windings, and the DC losses within are calculated analytically.
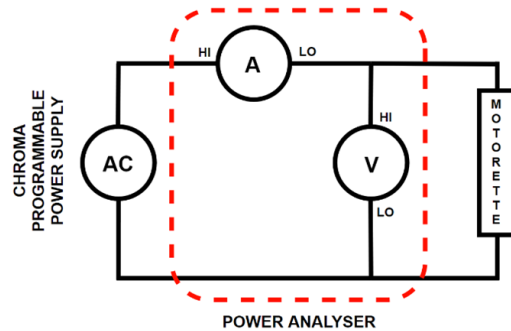

Figure 5. Schematic diagram of the experimental setup showing the AC source, the power analyser and the motorette inserted.
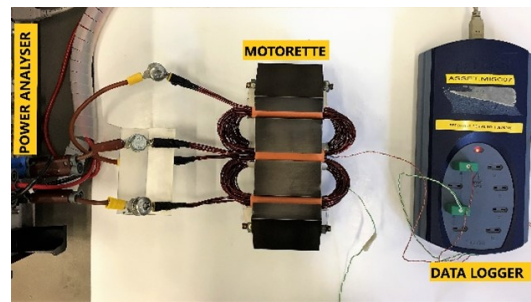

Figure 6. Actual experimental setup showing the power analyser, the motorette and the data logger for reading temperature inside the slot.
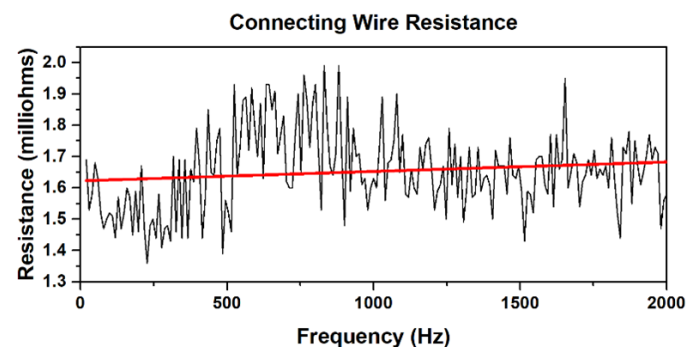

Figure 7. Measured AC resistance of the connecting wire against the frequency.

3. Comparison of FEA and Experimental Results

Table 3 shows the comparison of the FEA calculated loss and the experimentally measured loss of the motorette. The losses measured at 20 Hz are considered as DC values. Here, the column 'Active length Loss' represents the 2D-FEA-computed winding loss (only the windings within the machine's stator stack were considered, i.e., not including the end-windings). The column 'Total Sim. Loss' represents the active length loss added with the I^2R loss of the auxiliary components (lead wires, crimp contacts, connecting cables), end-winding DC loss component and the core loss as computed from FEA. The column 'Total Exp. Loss' represents the total experimentally measured loss of the motorette setup (with the auxiliary components connected). The column '% difference' represents the percentage difference between the 'Total Simulated Loss' and the 'Total Experimental Loss'. The simulated and experimental total losses match well, with the maximum difference being 9.7% at the measured frequency of 1000 Hz. Finally, the column 'Total/DC loss

(experimental)' represents the ratio of total experimentally measured loss minus the 2D-FEA computed core loss at high frequency to the total experimentally measured DC loss of the setup.

Table 3. Comparison of FEA calculated loss and experimental measured loss.

Freq. (Hz)	Active Length Loss (W)	Total Sim. Loss (W)	Total Exp. Loss (W)	% Difference	Total/DC Loss (Experimental)
DC	9.74	29.06	30.2	3.92	1
50	9.75	29.14	29.71	1.96	1.06
100	9.79	29.26	31.35	7.14	1.22
200	9.92	29.61	30.27	2.23	1.08
500	10.85	31.45	32.44	3.15	1.19
666.67	11.71	32.91	34.61	5.17	1.24
1000	14.13	36.89	40.47	9.70	1.51
1500	19.42	45.08	48.99	8.67	1.65

4. Comparison of Fixed Strands Positions and Fixed Conductor Shapes

For the purpose of this experimental analysis, two winding cases were considered: (a) fixed strands' positions (CASE A) and (b) fixed conductors' shapes (CASE B). For CASE A, the results of the motorette described in the previous section were used. For CASE B, the conductors' shapes of the motorette CASE A were kept fixed, and 3D-printed slot formers were manufactured. Figure 8 shows the conductors' shape in motorette CASE A (strand position controlled) and the corresponding slot formers for CASE B, where the strand positions are not controlled but the overall strand grouping (conductor) follow the shape patterns of CASE A. For CASE B, the same parameters were used as in CASE A such as magnet wire size, number of turns, strands-in-hand, etc., Figure 9 shows the formers and motorette with fixed conductor shapes (CASE B).
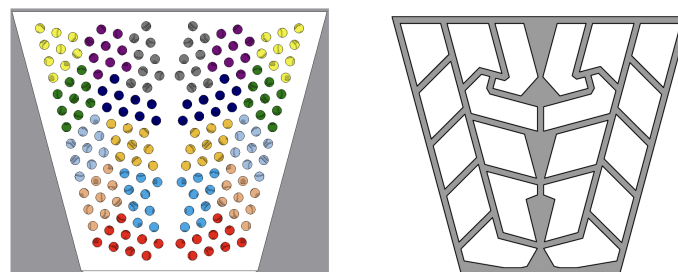

Figure 8. Strands' positions and conductors' shapes: (**Left**) CASE A; (**Right**) CASE B.
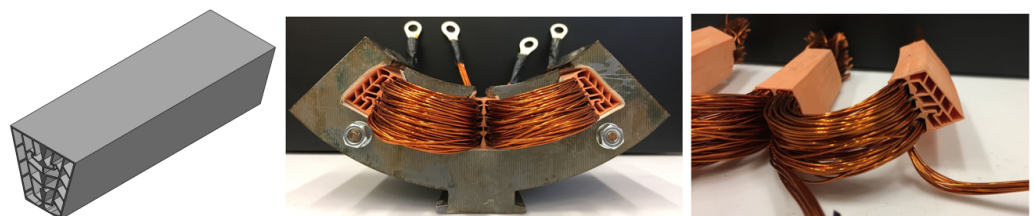

Figure 9. Formers and motorette with fixed conductors' shape (CASE B); (**Left**) 3D rendering of the slot former, (**Centre**) wound motorette with the slot former, (**Right**) winding in the slot former.

Table 4 lists the comparison of the measured total losses in the motorette CASE A and CASE B. The columns 'Measured total loss (W)' represent the total measured losses of the motorette for CASE A and CASE B against the frequencies listed in the first column 'Frequency (Hz)'. These measured losses include all the losses of the motorette setup, i.e., the winding losses, the DC losses of the connecting wires and lead wires and the core loss in the motorette. The columns 'Losses in winding' lists the losses in the winding for

both the cases. Here, the losses in the winding are calculated by subtracting the core loss calculated using the FEA from the measured total losses of the motorettes. The results for 'Losses in the winding' also include the DC losses in the connecting cables, lead wires and the end-windings. The columns 'Total/DC loss ratio (winding)' show the Total/DC loss ratio in the winding for both motorette cases. The measurements taken at 20 Hz are considered as DC values. Hence, the ratio of the losses in the winding at any frequency by the losses in the winding at 20 Hz gives the Total/DC loss ratio. Finally, the column '% difference' shows the percentage difference between the Total/DC loss ratio of CASE B and CASE A.

Table 4. Comparison of losses in motorette CASE A and CASE B.

Freq. (Hz)	Measured Total Loss in CASE A (W)	Measured Total Loss in CASE B (W)	Losses in Winding CASE A (W)	Losses in Winding CASE B (W)	Total/DC Loss (Winding) CASE A	Total/DC Loss (Winding) CASE B	% Difference
20	30.20	25.09	30.17	25.07	1.00	1.00	0.00
50	29.71	25.08	29.64	25.01	0.98	1.00	1.58
100	31.35	25.37	31.19	25.21	1.03	1.01	−2.70
500	32.43	26.21	31.15	24.93	1.03	0.99	−3.66
666.67	34.60	28.26	32.69	26.35	1.08	1.05	−2.97
1500	48.98	38.60	42.64	32.26	1.41	1.29	−8.93

The results from this comparison of motorette CASE A and CASE B are closely matched. The maximum difference occurs at the frequency of 1500 Hz, where the losses in CASE B drop by approximately 9% compared to CASE A. It is suspected that for the fixed conductor shapes (CASE B) a degree of transposition inadvertently occurs due to axial strand displacement which helps reduce the losses. The comparison of CASES A and B suggests that the positions of the individual strands are not vital as long as the shapes of the conductors are maintained. Compared to [18], this radically simplifies and accelerates the winding process, providing a simpler solution to minimize the AC losses.

5. Relationship between AC Losses and Copper Filling Factor

For this subsequent experimental analysis, the slots in the motorette were randomly wound while increasing the slot copper filling factor (CFF) in three steps, 20%, 30% and 40%, respectively. The AC losses in the winding of the motorette for each of the three cases were measured, and finally the results were compared to the results obtained using the motorette with 33 'strands–in–hand' which corresponds to the strand size and number of parallel strands in the actual traction machine.

Table 5 lists the comparisons of the specifications in the slots of motorettes with the varying copper filling factor as well as the specifications in the slot of the motorette with 33 'strands-in-hand'. For the motorette cases with copper filling factor of 20%, 30% and 40%, the strand diameter and the numbers of turns are kept constant. So, as the copper filling factor changes, the number of parallel strands or 'strands-in-hand' of a conductor change accordingly. The last column '44.5%' shows the specifications of the motorette with 33 'strands-in-hand'. Here, the strand diameter of 0.63 mm is being used so as to be identical with the existing traction machine of Table 1. Figure 10 shows the randomly-wound experimental motorettes.

Table 5. Specifications in the slot for motorettes with varying copper filling factor (CFF).

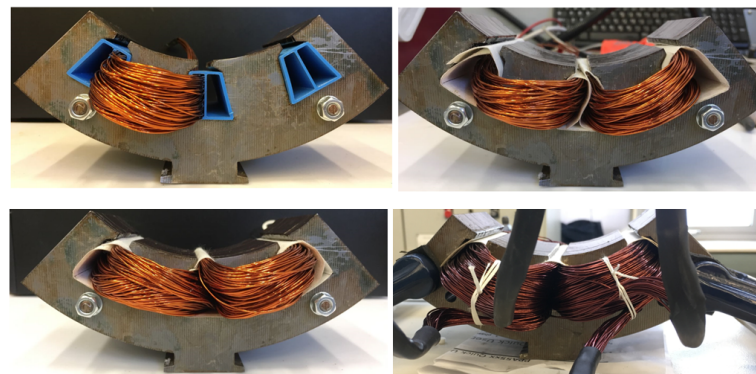| Parameter	Motorette with CFF 20%	Motorette with CFF 30%	Motorette with CFF 40%	Motorette with CFF 44.5%
Turns per half slot	10	10	10	10
Strands-in-hand	9	14	18	33
Strand diameter (mm)	0.8	0.8	0.8	0.63
Total strands per slot	180	280	360	660
Strand Copper diameter (mm)	0.8	0.8	0.8	0.63
Nominal Current Density (A/mm^2)	6.63	4.26	3.31	2.91

Figure 10. Experimental motorettes with varying CFF: (**Top Left**) 20% CFF; (**Top Right**) 30% CFF; (**Bottom Left**) 40% CFF; and (**Bottom Right**) motorette with 33 'strands-in-hand'.

Table 6 lists the comparison of the losses in the motorettes and the Total/DC loss ratio in the winding for the three CFF considered. In Table 6, the columns under 'Measured Total Losses (W)' represent the measured total losses in the motorette for the CFF for different frequencies supplied. The columns under 'Losses in Winding' represent the losses in the winding. This includes the losses in the auxiliary components (considered as DC losses), i.e., the losses in the end-winding, the connecting cables and the lead wires. The 'Losses in Winding' are calculated by subtracting the core loss value calculated using FEA from the measured total loss of the motorette at the different frequencies. The columns under Total/DC Loss (Winding) represent the Total/DC loss ratio in the windings. Again, the losses at 20 Hz are considered as baseline DC loss values.

Table 6. Comparison of losses in the motorettes with varied copper filling factor.

Freq. (Hz)	Measured Total Loss 20% CFF (W)	Measured Total Loss 30% CFF (W)	Measured Total Loss 40% CFF (W)	Losses in Winding 20% CFF (W)	Losses in Winding 30% CFF (W)	Losses in Winding 40% CFF (W)	Total/DC Loss (Winding) 20% CFF	Total/DC Loss (Winding) 30% CFF	Total/DC Loss (Winding) 40% CFF
20	24.28	19.95	15.64	24.26	19.93	15.62	1.00	1.00	1.00
50	24.32	20.50	15.95	24.25	20.43	15.88	1.00	1.03	1.02
100	24.32	20.56	16.63	24.17	20.41	16.48	1.00	1.02	1.05
500	26.31	22.44	19.42	25.03	21.16	18.14	1.03	1.06	1.16
666.67	27.65	23.96	20.79	25.74	22.04	18.87	1.06	1.11	1.21
1500	39.31	36.87	35.05	32.97	30.53	28.71	1.36	1.53	1.84

This experimental result analysis shows that at lower frequencies the relationship between the CFF and AC losses in the winding is insignificant. However, at high frequencies (>500 Hz), as the CFF increases the AC losses in the winding increase. For instance, when the supplied frequency is 1500 Hz, the Total/DC loss ratio in the windings with 40% CFF is approximately 35% higher than the Total/DC loss ratio with 20% CFF. While in the presented cases the higher filling factor still yields the lowest net losses, it can be clearly

deduced from the experimental measurements that for machines operating most of the time at high frequencies it may well be more efficient/economical to use a lower CFF.

Figure 11 shows the comparison of the Total/DC loss ratio in the winding for 20%, 30% and 40% CFF along with the Total/DC loss ratio in the winding of the 33 'strands-in-hand' motorette, which corresponds to the actual motor. For the motorette with 33 'strands-in-hand', the total losses in the winding are 80 W when the frequency is 1200 Hz. In addition, when compared to the 40% CFF, the motorette with 33 'strands-in-hand' has a CFF of 44.5%, which is 11.25% higher. However, with a smaller strand diameter, the total/DC loss ratio is approximately 4.42 when the supply frequency is 1200 Hz compared to 1.7 for the motorette with 18 thicker 'strands-in-hand'. This is due to the greater circulating current effects in the motorette with the higher number of thinner parallel strands.
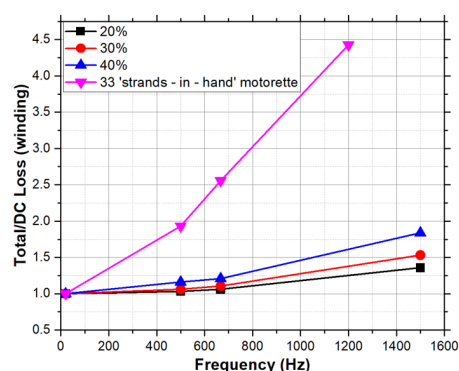

Figure 11. Comparison of Total/DC Loss ratio of the motorettes.

6. Segregation of Losses

The losses in the winding can be segregated as DC loss, skin and proximity (strand level) loss and circulating current (bundle level) loss. It can be represented as:

$$P_{Total} = P_{DC} + P_{skin\ and\ proximity} + P_{circulating\ current} \tag{1}$$

To study the individual contribution of the loss components, three arrangements of bundles are considered, namely: (a) ARR1, (b) ARR2 and (c) ARR3 as shown in Figure 12. Here, each colour represents a bundle, and strands of the same colour represent strands-in-hand of each bundle. To eliminate the bundle level losses (at simulation level) arising from circulating currents in the bundle, each strand is supplied with its own current source to guarantee even distribution, as shown in Figures 13 and 14. Figure 15 shows the current density (J) comparison at a given instant of time for the models with a single supply source and multi-source supply connected to each individual strand. It is evident from Figure 15 that the circulating current effect can be minimized/eliminated at simulation level by this approach. Thus, the DC, the skin and the proximity effect (strand level) components of the winding loss are dominant in multi-source current analysis.

Using this methodology, the losses are segregated into their constituent components. Figure 16 shows the comparison of segregated losses for the three aforesaid bundle arrangements. The strand level loss component (skin and proximity effect loss) remains nearly identical. However, the bundle level loss (circulating current loss) is greatly influenced by the shape of the bundle. This is caused by the distribution of leakage flux inside the slot and uneven flux linkage by the strands-in-hand.
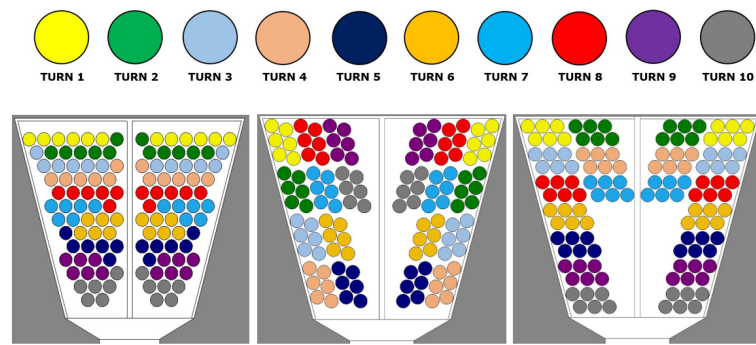
Figure 12. The configuration of strands and bundles in the slot as: (**Left**) horizontal (ARR1); (**Centre**) vertical bundled (ARR2); (**Right**) horizontal bundled (ARR3).
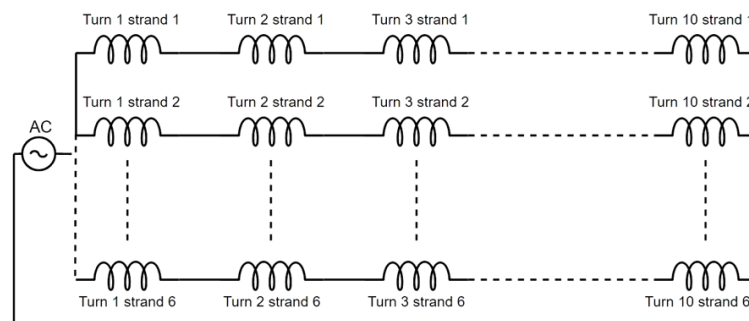

Figure 13. Circuital representation of the strands and bundle connections in the models with a single supply source.
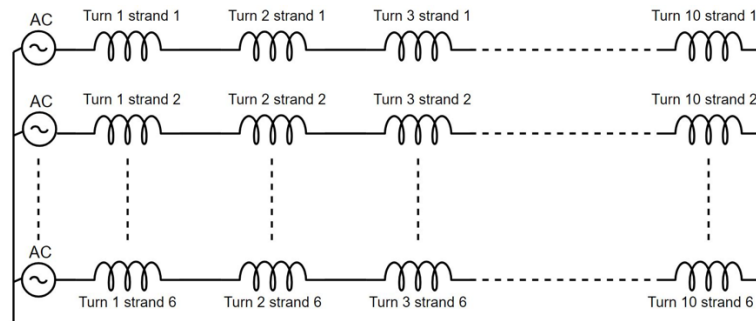

Figure 14. Circuital representation of the strands and bundle connections in the models with multiple supply sources, each connected to an individual strand.
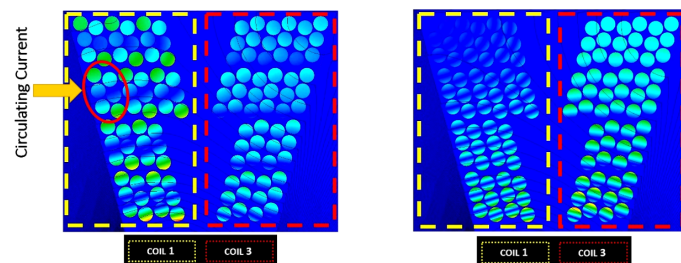

Figure 15. Comparison of current density (J) in the strands for the 24 parallel strands models (ARR2) at time instant (0.00194s): (**Left**) with circulating current; (**Right**) without circulating current.
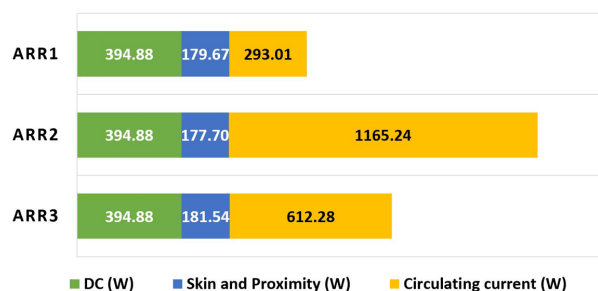
Figure 16. Segregation of losses in the winding into components for ARR1, ARR2 and ARR3.

7. Conclusions

High frequency AC losses in electric machines with non-transposed conductors are notoriously hard to predict and tricky to manage. This paper, which follows up from earlier research presented by the authors in [18], verifies experimentally that AC losses can be calculated with accuracy (less than 10% difference up to 1.5 kHz) if the strand positions in the slot are controlled to be at the same coordinates as the FEA model. With the aforementioned baseline verification established, it has been shown using experimental motorettes that the exact positions of the strands in a conductor are not vital as long as the conductor shapes maintain the desired shape. This is an important development to the authors' earlier work [18] showing that a simplified and easier to implement solution involving conductor shape control can still yield significant benefits in AC loss reductions. The solution proposed in this paper results in a significant reduction in the time required for winding a machine compared to the solution in [18]. Although an EV machine with concentrated type winding was used as basis of the analyses, the loss mitigation technique presented is applicable to all high frequency machines using mush winding (concentrated or distributed winding). The analyses presented in both [18] and this paper are at a lower technology readiness level. However, with the advancement of 3D printing technology, the solutions can be improved towards a higher technology readiness level (TRL). In fact, controlling the bundle shape instead of the individual strand position is a significant simplification to the process of winding a machine. Adding a slot former reduces the effective copper fill factor and increases the DC component of the winding loss. The addition of a slot former also results in the increase of the component number in manufacturing the machine. However, given the lower TRL status of the proposed solution at this stage, an economic analysis at the level of high volume applications as suggested in the Advanced Propulsion Centre roadmap for electric machines [28] should be performed. In the design of an electric machine, maximising the copper slot-filling factor is traditionally proposed to reduce losses in the winding. Using random-wound motorettes with varying copper filling factors and strand diameters, it has been experimentally shown that for high frequency machines (>1 kHz), counter-intuitive design choices such as using a lower copper fill factor and thicker strand diameters may be beneficial in achieving the highest overall efficiency. Finally, segregation of the winding losses into its individual components is shown at the simulation level.

Author Contributions: Conceptualization, A.B., D.G., M.D. and C.G.; methodology, A.B., D.G., T.Z. and M.D.; software, A.B.; validation, D.G., M.D., T.Z., C.Z. and C.G.; formal analysis, A.B.; investigation, A.B., T.Z., D.G. and C.Z. resources, C.G.; data curation, A.B.; writing—original draft preparation, A.B.; writing—review and editing, D.G., M.D. and T.Z.; visualization, A.B.; supervision, D.G., M.D. and C.G. All authors have read and agreed to the published version of the manuscript.

Data Availability Statement: The data presented in this study are available on request from the corresponding author. The data are not publicly available due to privacy.

Conflicts of Interest: The authors declare no conflict of interest.

Abbreviations

The following abbreviations are used in this manuscript:

R&D   Research and Development
DoE   Department of Energy
FEA   Finite Element Analysis

References

1. A Technical Summary of Euro 6/VI Vehicle Emission Standards. Available online: https://theicct.org/sites/default/files/publications/ICCT_Euro6-VI_briefing_jun2016.pdf (accessed on 12 June 2022).
2. Popescu, M. Electrical Vehicles—Practical Solutions for Power Traction Motor Systems. *IEEE Trans. Ind. Appl.* **2018**, *54*, 2751–2762. [CrossRef]
3. Gerada, D. High-Speed Electrical Machines: Technologies, Trends, and Developments. *IEEE Trans. Ind. Electron.* **2014**, *61*, 2946–2959. [CrossRef]
4. Schiefer, M.; Doppelbauer, M. Indirect slot cooling for high-power-density machines with concentrated winding. In Proceedings of the 2015 IEEE International Electric Machines Drives Conference (IEMDC), Coeur d'Alčne, Idaho, 10–13 May 2015; pp. 1820–1825.
5. Vetuschi, M. Minimization of Proximity Losses in Electrical Machines with Tooth-Wound Coils. *IEEE Trans. Ind. Electron.* **2015**, *51*, 3068–3076. [CrossRef]
6. L-Refaie, A.M.E. Fractional-Slot Concentrated-Windings Synchronous Permanent Magnet Machines: Opportunities and Challenges. *IEEE Trans. Ind. Electron.* **2010**, *57*, 107–121. [CrossRef]
7. Barcaro, M. Design and Analysis of Interior Permamnet Magnet Synchronous Machines for Electric Vehicles. Ph.D. Thesis, University of Padova, Padova, Italy, 2011
8. Boldea, I. Automotive Electric Propulsion Systems With Reduced or No Permanent Magnets: An Overview. *IEEE Trans. Ind. Electron.* **2014**, *61*, 5696–5711. [CrossRef]
9. Golovanov, D. Multidomain Optimization of High-Power-Density PM Electrical Machines for System Architecture Selection. *IEEE Trans. Ind. Electron.* **2018**, *65*, 5302–5312. [CrossRef]
10. Mellor, P.H.; Wrobel, R.; McNeill, N. Investigation of Proximity Losses in a High Speed Brushless Permanent Magnet Motor. In Proceedings of the Conference Record of the 2006 IEEE Industry Applications Conference Forty-First IAS Annual Meeting, Tampa, FL, USA, 8–12 October 2006.
11. Van Der Geest, M.; Polinder, H.; Ferreira, J.A.; Zeilstra, D. Stator winding proximity loss reduction techniques in high speed electric machines. In Proceedings of the Conference Record of the 2013 International Electric Machines Drives Conference, Chicago, IL, USA, 12–15 May 2013; pp. 340–346
12. Mellor, P.; Wrobel, R.; Salt, D.; Griffo, A. Experimental and analytical determination of proximity losses in a high-speed PM machine. In Proceedings of the 2013 IEEE Energy Conversion Congress and Exposition, Denver, CO, USA, 15–19 September 2013; pp. 3504–3511.
13. Popescu, M.; Dorrell, D.G. Proximity Losses in the Windings of High Speed Brushless Permanent Magnet AC Motors With Single Tooth Windings and Parallel Paths. *IEEE Trans. Magn.* **2013**, *49*, 3913–3916. [CrossRef]
14. Reddy, P.B.; Zhu, Z.Q.; Han, S.; Jahns, T.M. Strand-level proximity losses in PM machines designed for high-speed operation. In Proceedings of the 2008 18th International Conference on Electrical Machines, Vilamoura, Portugal, 6–9 September 2008; pp. 3504–3511.
15. Reddy, P.B.; Jahns, T.M.; Bohn, T.P. Transposition effects on bundle proximity losses in high-speed PM machines. In Proceedings of the (ECCE), San Jose, California, 20–24 September 2009; pp. 1919–1926.
16. Reddy, P.B.; Jahns, T.M.; Bohn, T.P. Analysis of bundle losses in high speed machines. In Proceedings of the The 2010 International Power Electronics Conference-ECCE ASIA-(IPEC-Sapporo 2010), Sapporo, Japan, 21–24 June 2010; pp. 2181–2188.
17. Reddy, P.B.; Jahns, T.M.; Bohn, T.P. Modeling and analysis of proximity losses in high-speed surface permanent magnet machines with concentrated windings. In Proceedings of the 2010 IEEE Energy Conversion Congress and Exposition (ECCE 2010), Atlanta, GA, USA, 12–16 September 2010; pp. 996–1003.
18. Bardalai, A. Reduction of Winding AC Losses by Accurate Conductor Placement in High Frequency Electrical Machines. *IEEE Trans. Ind. Electron.* **2020**, *56*, 183–193. [CrossRef]
19. Atkinson, G.J. The Analysis of Losses in High-Power Fault-Tolerant Machines for Aerospace Applications. *IEEE Trans. Ind. Electron.* **2006**, *42*, 1162–1170. [CrossRef]
20. Iwasaki, S. Influence of PWM on the Proximity Loss in Permanent-Magnet Brushless AC Machines. *IEEE Trans. Ind. Electron.* **2009**, *45*, 1359–1367. [CrossRef]

21. Thomas, A.S.; Zhu, Z.Q.; Jewell, G.W. IProximity Loss Study In High Speed Flux-Switching Permanent Magnet Machine. *IEEE Trans. Magn.* **2009**, *45*, 4748–4751. [CrossRef]
22. Mellor, P.; Wrobel, R.; Simpson, N. AC losses in high frequency electric machine windings formed from large section conductors. In Proceedings of the 2014 IEEE Energy Conversion Congress and Exposition (ECCE), Pittsburgh, PA, USA, 14–18 September 2014; pp. 5563–5570.
23. Gyselinck, J. Homogenization of Form-Wound Windings in Frequency and Time Domain Finite-Element Modeling of Electrical Machines. *IEEE Trans. Magn.* **2010**, *46*, 2852–2855. [CrossRef]
24. Sullivan, C.R. Optimal choice for number of strands in a litz-wire transformer winding. *IEEE Trans. Power Electron.* **1999**, *14*, 283–291. [CrossRef]
25. Tang, X.; Sullivan, C.R. Stranded wire with uninsulated strands as a low-cost alternative to litz wire. In Proceedings of the IEEE 34th Annual Conference on Power Electronics Specialist, 2003. PESC '03, Acapulco, Mexico, 15–19 June 2003; pp. 1919–1926.
26. Hämäläinen, H.; Resistance, A.C. Factor of Litz-Wire Windings Used in Low-Voltage High-Power Generators. *IEEE Trans. Ind. Electron.* **2014**, *61*, 693–700. [CrossRef]
27. Nan, X.; Sullivan, C.R. An Equivalent Complex Permeability Model for Litz-Wire Windings. *IEEE Trans. Ind. Appl.* **2009**, *45*, 854–860. [CrossRef]
28. Advanced Propulsion Centre Roadmap 2020: Electrical Machines. Available online: https://www.apcuk.co.uk/media-type/roadmaps/ (accessed on 12 June 2022).